PHYSICS

Frenkel biexcitons in hybrid HJ photophysical aggregates

Elizabeth Gutiérrez-Meza[1], Ravyn Malatesta[1], Hongmo Li[2], Ilaria Bargigia[3], Ajay Ram Srimath Kandada[3], David A. Valverde-Chávez[1], Seong-Min Kim[2], Hao Li[4], Natalie Stingelin[2,5], Sergei Tretiak[6], Eric R. Bittner[4]*, Carlos Silva-Acuña[1,2,7]*

Frenkel excitons are unequivocally responsible for the optical properties of organic semiconductors and are predicted to form bound exciton pairs (biexcitons). These are key intermediates, ubiquitous in many photophysical processes such as the exciton bimolecular annihilation dynamics in such systems. Because of their spectral ambiguity, there has been, to date, only scant direct evidence of bound biexcitons. By using nonlinear coherent spectroscopy, we identify here bound biexcitons in a model polymeric semiconductor. We find, unexpectedly, that excitons with interchain vibronic dispersion reveal intrachain biexciton correlations and vice versa. Moreover, using a Frenkel exciton model, we relate the biexciton binding energy to molecular parameters quantified by quantum chemistry, including the magnitude and sign of the exciton-exciton interaction the intersite hopping energies. Therefore, our work promises general insights into the many-body electronic structure in polymeric semiconductors and beyond, e.g., other excitonic systems such as organic semiconductor crystals, molecular aggregates, photosynthetic light-harvesting complexes, or DNA.

INTRODUCTION

The primary photoexcitations in organic semiconductors are molecular electronic singlet states (S_1) termed Frenkel excitons (1). Although these states are localized within a chromophore, at sufficiently high densities, exciton-exciton interactions start to dominate the optical properties of organic solids (2). For example, the spontaneous formation of strongly coupled light-matter quantum condensates in organic materials depends fundamentally on the details of exciton-exciton interactions (3). Similarly, in biological light-harvesting complexes, multiexciton interactions may play important roles (4), while biexcitons can be crucial in cascade quantum emitters as a source of entangled photons (5). To fundamentally understand these processes, the molecular basis for biexciton stability needs to be established to provide a crucial comprehension of important structure/property interrelations that go beyond that achieved by examining single-quantum photoexcitations. While excitons deliver an important window into electronic dispersion and its dependence on macromolecular structure and configuration, biexcitons provide a sophisticated probe of electronic structure because they are consequential intermediates in a wide range of photophysical processes such as exciton dissociation into electrons (e^-) and holes (h^+) [$S_0 + 2\hbar\omega \longrightarrow [2\,S_1]^{\ddagger} \longrightarrow 2e^- + 2h^+$] ($6$), bimolecular annihilation [$S_1 + S_1 \longrightarrow [2\,S_1]^{\ddagger} \longrightarrow S_0 + S_0$] ($7$), and singlet fission producing triplet (T_1) states [$S_0 + 2\,\hbar\omega \longrightarrow [2\,S_1]^{\ddagger} \longrightarrow T_1 + T_1$] ($8$). The work in ($7$) notes that bimolecular annihilation may be mediated both by resonance energy transfer and

diffusion-limited exciton-exciton scattering, but in either case, we invoke the key intermediate $[2\,S_1]^{\ddagger}$.

While ample theoretical work points toward the existence of biexcitons in organic solids (9–15) and in optical lattices (16), there has been only indirect evidence of the dynamic formation of two-quantum exciton states in polymeric semiconductors by incoherent, sequential ultrafast excitation (6–8), in addition to a report on the indirect observation of such species in a molecular aggregate (17) and a conjugated polymer (18). The reason is that the spectroscopic signatures of Frenkel biexcitons in organic semiconductors have thus far been ambiguous, in strong contrast to Wannier-Mott biexcitons in quantum-confined semiconductor systems (19, 20). We note that Frenkel biexcitons have directly been observed in solid argon (21).

Here, we report the direct spectroscopic observation of bound Frenkel biexcitons, i.e., bound two-exciton quasiparticles ($[2\,S_1]^{\ddagger}$), in a model polymeric semiconductor, [poly(2,5-bis(3-hexadecylthiophene-2-yl)thieno[3,2-b]thiophene) (PBTTT)] (22). This allows us to quantify biexciton binding energies. We selected PBTTT because of its thermotropic phase behavior, hosting liquid-crystalline phases at temperatures above ambient conditions (23, 24), which, we expect, renders the disordered energy landscape highly dynamic. Notably, we identify a spectral structure that is obscured within the inhomogeneously broadened linear excitation line shape, which reflects both attractive and repulsive biexciton correlations and can be rationalized on the basis of microscopic criteria. For this, we develop a Frenkel exciton model that quantifies how the balance of (i) exciton-exciton correlation energy, (ii) the energetic variations between different sites in the polymer aggregate, and (iii) exciton delocalization defines biexciton stability.

RESULTS

In photophysical aggregates of semiconductor polymers, Frenkel excitons consist of chromophoric photoexcitations localized over at most a few subunits both along the polymer chain (categorized as a J-aggregate) and between multiple polymer chains (H-aggregate)

[1]School of Chemistry and Biochemistry, Georgia Institute of Technology, 901 Atlantic Drive, Atlanta, GA 30332, USA. [2]School of Materials Science and Engineering, Georgia Institute of Technology, North Avenue, Atlanta, GA 30332, USA. [3]Department of Physics and Center for Functional Materials, Wake Forest University, 1834 Wake Forest Road, Winston-Salem, NC 27109, USA. [4]Department of Chemistry, University of Houston, Houston, TX 77204, USA. [5]School of Chemical and Biomolecular Engineering, Georgia Institute of Technology, 311 Ferst Drive NW, Atlanta, GA 30332, USA. [6]Theoretical Division and Center for Nonlinear Studies, Los Alamos National Laboratory, Los Alamos, NM 87545, USA. [7]School of Physics, Georgia Institute of Technology, 837 State Street, Atlanta, GA 30332, USA.
*Corresponding author. Email: ebittner@central.uh.edu (E.R.B.); carlos.silva@gatech.edu (C.S.-A.)

(25), in many cases leading to hybrid HJ structures (26). Since the transition moment is typically oriented parallel to the polymer chains and therefore interacts in a head-to-tail fashion, J-aggregate excitons have a negative intrachain intersite hopping integral t_{intra}, which is directly related to the free-exciton bandwidth $W = 4|t_{intra}|$

and is inversely related to the exciton effective mass $t_{intra} = -\hbar^2/2\mu_{eff}$. Therefore, t_{intra} determines exciton delocalization. In contrast to J-aggregates, H-aggregates feature a positive t_{inter}. Both states (H- and J-aggregate states) are depicted in Fig. 1, which shows the potential scenarios for biexciton interactions between pairs of excitons. [We
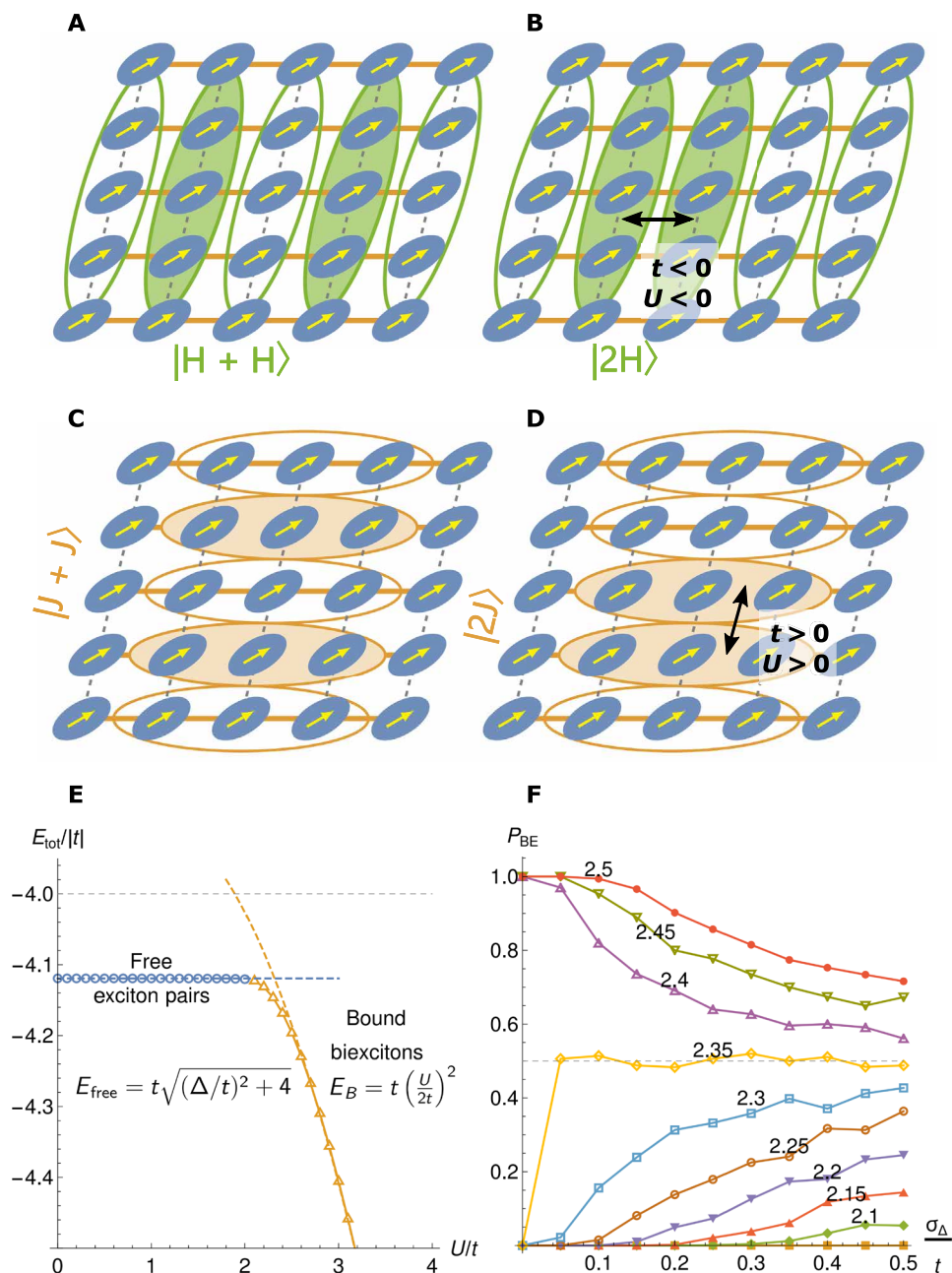
Fig. 1. Theoretical model for biexciton formation. (**A** to **D**) H versus J biexciton configurations. In (A) and (B), H-like excitons are delocalized along the π-stacking direction of the polymer chains and move along the chain with hopping integral $t < 0$. Here, exciton dipoles are aligned to produce an attractive $U < 0$ contact interaction. In comparison, the J-like excitons depicted in (C) and (D) move between chains with $t > 0$, and exciton dipoles are aligned cofacially to produce a repulsive $U > 0$ contact interaction. (**E**) Free versus bound biexciton energies. The energy of a free pair of excitons E_{free} is determined by their bandwidth, whereas the binding energy E_B is determined by the contact interaction U. Bound biexcitons become stable once $E_B < E_{free}$. Points correspond to energies from numerical diagonalization, while dashed curves are the asymptotic limits. The gray dashed line is for two free excitons on a homogeneous lattice ($\Delta = 0$). (**F**) Probability for biexciton formation for energetically disordered lattices. Here, we set $\Delta/t = 1$ and increase the variance in the local site energy. Curves are labeled by the interaction U for $U/t = 2.5$ to $U/t = 2.1$.

note that t_{intra}, t_{inter}, and the exciton hopping term $t_{2Q, intra (inter)}$ associated with exciton-exciton binding are a priori distinct; intra- and interchain exciton hopping terms certainly differ because of effects such as dipole-dipole orientation, charge-transfer contributions, and superexchange interactions, as do the corresponding hopping terms required for two-quantum binding. Within the effectively one-dimensional (1D) model discussed below, we will denote the hopping integral simply as t.] The small ellipsoids represent the molecular subunits, while the larger ellipsoids represent single electron/hole excitons delocalized over multiple sites either between chains (Fig. 1, A and B) or along the chains (Fig. 1, C and D). The latter of these form a quantum mechanical basis for biexciton formation.

Exciton pairs become bound when their mutual attraction overcomes both the energy barrier imposed by local energetics and their relative kinetic energy. However, there is a subtlety concerning the hopping integral t and the energy strength of the exciton-exciton contact interaction U. These parameters must have the same signs to produce a bound species. We note that both attractive and repulsive interactions can produce bound states. Ordinarily, we set $t < 0$ and $U < 0$ producing a single state that is energetically below twice the exciton state. However, bound states can also occur when $t > 0$ and $U > 0$. These states would occur at the top of the energy band for free biexcitons. We further discuss this in the Supplementary Materials.

Curiously, H-aggregate excitons can move parallel to the chains with transfer integral $t < 0$. Moreover, the orientation of the local exciton dipoles gives $U < 0$, implying that H-like exciton pairs can form bound biexcitons with an attractive binding energy below that of the energy for free H-like exciton pairs. On the contrary, J-like excitons can move perpendicular to the chains with transfer integral $t > 0$ and with contact interaction $U > 0$. This implies that the bound J-like biexciton states can form above the continuum for free J-like exciton pairs. Because of the hybrid HJ aggregate nature (26) established in PBTTT (27), both H-like and J-like behavior can be found offering the possibility of observing both 2J and 2H biexcitons within the same system.

Additional insights can be gained considering that, in a many-body framework, the exciton-exciton binding physics can be captured with a 1D Hubbard-like model with contact interaction, U, between occupied nearest neighbors along the 1D chain. The hybrid HJ aggregate lattice is inherently 2D, and it is possible that mixing between H-like and J-like excitons contributes to the formation of bound two-quantum quasiparticles. However, for the purposes of the analysis of this paper, we assume that the most important states for biexciton binding will involve the states with the longest and shortest wave vectors in each direction. On the basis of this reasonable assumption, we can reduce the full 2D model to 1D by assuming separability of the single exciton motion between motion along and perpendicular to the polymer chains and then introducing the exciton-exciton interactions. Introducing energetic disorder either into the local site energies or into the hopping integrals will break this separability and induce mixing between the H- and J-like excitons. However, we assume that this mixing will be primarily within the bulk of the density of states and have modest impact (depending of course on the relative magnitude of the disorder) on the extremal states corresponding to the bound biexcitons. Hence, we argue that the 1D model captures the salient physics and provides the correct theoretical framework for interpreting and understanding the observations. We describe the Hamiltonian in the Supplementary Materials along with its reduction from a more general 2D model implied by Fig. 1. This model, on the one hand, accounts for energetic differences between repeating units, $\pm\Delta$, which we refer to as the crenelation. Although this effect gives rather artificial alternating site variations in energies, it is illustrative in that it captures the effects of disorder. For dissociated pairs, we can ignore the contact interaction and set $U = 0$ to obtain the ratio of noninteracting excitons E_{free} and the intersite hopping integral t, $E_{free}/t = 2\sqrt{(\Delta/t)^2 + 4}$, as the limiting case for two excitons with bulk momentum $k = 0$. On the other hand, the contact potential produces a single bound biexciton state with binding energy of $E_b/t = (U/2t)^2$. Exciton pairs are bound once $E_b < E_{free}$ (for the 2J). This gives the insights that the critical value of the coupling varies as Δ^2. Hence, crenelation destabilizes the exciton binding, suggesting that a highly crenelated lattice would disfavor biexciton binding. Figure 1E shows the two asymptotic limits of our model given as dashed curves, which results from a numerically exact diagonalization of a two-band Hubbard-like Hamiltonian. For our numerical studies, we set both $U < 0$ and $t < 0$ so that the bound 2H biexciton is found at the bottom of the energy spectrum. The 2J case is identical except for a sign change in the energy axis, producing a bound 2J state at the top of the energy spectrum (see the Supplementary Materials for additional details).

Another important point to take into account is that polymers are inherently heterogeneous systems. As a consequence, polymeric
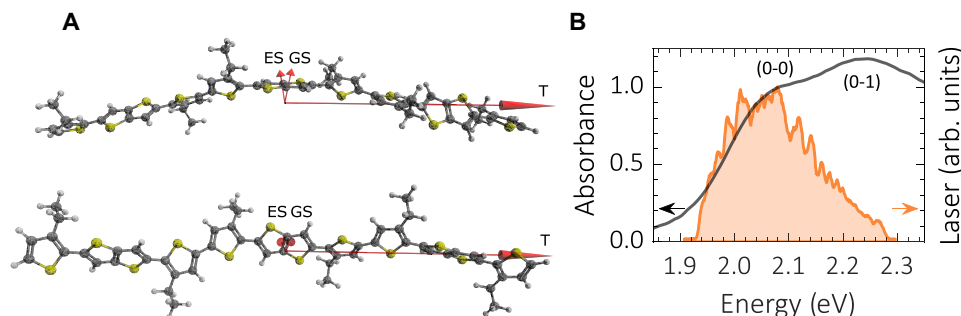
Fig. 2. Photophysical structure of PBTTT. (**A**) Calculated orientation of the transition dipole moment (T), as well as the ground- and excited-state dipoles (GS and ES) for a trimer, for the particular configuration shown here. The angle of the ground-state dipole with respect to the transition dipole is 79.3° and that for the excited-state dipole is 99.5°. The amplitudes of the ground state, excited state, and transition dipole moment are 0.98, 0.93, and 18.29 D, respectively. The dipoles are not drawn to scale. (**B**) Linear absorption spectrum of PBTTT measured at 5 K. Superimposed is the spectrum of the femtosecond pulse train used for the measurements presented in Fig. 4.

semiconductors typically exhibit a disordered energy landscape, which is reflected as a random variation in the site energies in our model. To examine this, we write $\Delta_n = \bar{\Delta} + \delta\Delta_n$, where $\overline{\delta\Delta_n\delta\Delta_{n'}} = \sigma_\Delta^2\delta_{nn'}$ gives the variance for a normal distribution with $\overline{\delta\Delta_n} = 0$. Figure 1F shows the probability of biexciton formation (P_{BE}) for various values of the interaction strength U and for increasing levels of site-wise energy fluctuations σ_Δ (for $\Delta/t = 1$). The results indicate that bound biexcitons are robust against local energy disorder up to a certain point. Beyond this, energetic disorder destabilizes the bound biexciton state. However, we also note that for extremely weakly interacting excitons, local disorder can enhance the formation of bound pairs when U is close to the stability threshold. This can occur if neighboring sites have a fortuitously small enough energy offset to form a local trapping site for a bound biexciton. However, the line shape for these biexcitons will be broad to reflect the inhomogeneous distribution of their energies.

It is furthermore critical to emphasize that U will depend on the local exciton dipole moment. Figure 2A shows front and side views of the chemical structure of a PBTTT oligomer (three repeat units, a trimer) as optimized using density functional theory (DFT; B3LYP/6-31G* level). The figure also displays the direction of the $S_0 \rightarrow S_1$ transition dipole moment corresponding to the fundamental exciton state. The dipole, which is oriented along the long molecular axis, is large, corresponding to strong optical absorbance. Superimposed are the ground (S_0) and excited (S_1) state static dipoles, which have a small amplitude and are largely oriented perpendicular to the long molecular axis. These are highly sensitive to the instantaneous configurations adopted by the chain and average to zero over all chain conformations in the bulk system. Although the conformational average vanishes, variance about this average is significant and maps into the local site energy variance σ_Δ, thereby having an impact on the stability of multiexciton states.

Experimentally, we deduce from the linear spectral line shape of PBTTT a dominant H-aggregate character (Fig. 2B). The reason is that the peak at ~2.06 eV, which corresponds to the 0-0 vibronic peak, is suppressed with respect to the rest of the vibronic progression (26). This corresponds to the situation in Fig. 1A for a single exciton. By fitting the absorption spectrum shown in Fig. 2B to a modified Frank-Condon progression (28), we obtained the energy of the main intramolecular vibration $E_p = 179$ meV and $W = 4|t_{inter}| \approx 60$ meV, expressed via the 0-0/0-1 absorbance ratio (29) and thus that $t_{inter} \approx 15$ meV. We have previously demonstrated that predominantly J-aggregate character can be induced by blending the same material with polyethyleneoxide (27). The 0-0 absorbance peak red-shifts by ~70 to 80 meV in that case (see the Supplementary Materials for a comparison of the absorption line shape of this batch of PBTTT processed as predominantly H- and J-aggregates).

To address the challenge of quantifying the biexciton spectral structure, we performed coherent 2D photoluminescence excitation (2D-PLE) spectroscopy on PBTTT. These measurements can directly identify biexciton resonances via two-quantum coherences (see details in the Supplementary Materials). Thus, they can quantify the biexciton binding energies (19, 20). This requires the construction of the coherent 2D excitation spectrum via incoherent measurement of the time-integrated photoluminescence (PL) intensity due to a fourth-order excited-state population arising from the interference of wave packets produced by a sequence of four light-matter interactions (30), allowing the measurement of the spectral correlations between resonance involving pulses 1 and 2 and those corresponding

to pulses 3 and 4 in Fig. 3A. Thereby, the two energy axes are constructed by Fourier transformation of the 2D coherence decay function along time variables t_{21} and t_{43} at a fixed population time t_{32}. Accordingly, the spectral correlation along resulting energy axes ($\hbar\omega_{21}$, $\hbar\omega_{43}$) involves single-quantum ($|0\rangle \rightarrow |1\rangle$) and two-quantum ($|0\rangle \rightrightarrows |2\rangle$) transitions, represented schematically in the left of Fig. 3B. The two principal coherent pathways involving the correlations between one- and two-quantum coherences under this detection scheme are depicted by the double-sided Feynman diagrams in Fig. 3B. We also display schematic diagrams of the one- and two-quantum 2D-PLE coherent spectra for two correlated transitions in Fig. 3 (C and D, respectively). These may be correlated, for example, via a common ground state such as H-like and J-like states in an HJ aggregate, each evident in the diagonal of the 2D-PLE spectrum ($\hbar\omega_{21} = \hbar\omega_{43}$). In addition, the spectral correlation between these two peaks is manifested by cross peaks between the diagonal features. Similarly, in the two-quantum correlation spectrum, a signal along the two-quantum diagonal ($\hbar\omega_{21-2Q} = 2\hbar\omega_{43}$) signifies two noninteracting excitons, while a signal above or below the diagonal signifies binding interactions with repulsive or attractive character, depending on the signs of t and U (H- or J-like coupling), respectively. In our schematic in Fig. 3D, the lower-energy diagonal peak displays 2J biexcitons (the two-quantum energy is higher than twice the one-quantum energy), while the higher-energy resonance displays structure corresponding to 2H biexcitons (in which the two-quantum energy is less than twice the one-quantum energy).

We first focus on the single-quantum 2D-PLE line shape in Fig. 4A. We note that the spectral range of the measurement, limited by the femtosecond laser spectrum displayed in Fig. 2B, overlaps with the entire 0-0 absorption peak. The 2D spectrum is dominated by a symmetric diagonal peak centered at $\hbar\omega_{21} = \hbar\omega_{43} \approx 2.06$ eV, corresponding to the 0-0 peak energy. We also observe a weak diagonal signal centered at ~1.99 eV, with even weaker structure identified at lower energy. These features display intense cross peaks with the (0-0) resonance. The rich spectral structure displayed at the low-energy tail of the 2D-PLE spectrum is not evident in the featureless linear absorption spectrum (Fig. 2) since it is obscured by the inhomogeneous line shape and demonstrates the existence of distinct states at the low-energy edge of the 0-0 absorption peak. We note that the energy of the weak diagonal feature corresponds to the 0-0 absorbance peak energy found in PBTTT J-aggregates induced when blending this semiconductor with a polar commodity plastic (27). We thus hypothesize that these are weak signatures of J-aggregate macromolecular conformations bearing effects of interactions with static dipoles (Fig. 2A). We present in the Supplementary Materials the linear absorption spectrum of the same batch of PBTTT in a blend with an ionic liquid, processed such that the J-aggregate dominates the line shape, which supports our assignment in Fig. 4. The 0-0 absorption peak in that film is at 1.96 eV, consistent with the spectrum reported in (27), which supports the assignment of the weak, low-energy diagonal feature as the origin of the J-aggregate progression.

We next examine two-quantum correlations within the spectral structure in Fig. 4B, looking for exciton-exciton resonances that display repulsive or attractive biexciton binding energies as depicted in Fig. 3D. Most prominently, we observe a broad distribution along the two-quantum energy axis $\hbar\omega_{21,2Q}$ centered at the one-quantum energy $\hbar\omega_{43} = 2.06$ eV (the 0-0 excitation maximum), with the peak of the distribution below the two-quantum diagonal, i.e., below the

energy at which $\hbar\omega_{21,2Q} = 2\hbar\omega_{43}$. Thereby, the spectrum cuts through the diagonal line, with a tail extending to the high-energy side of the diagonal. We also observe two-quantum peaks for the features at lower energy than the 0-0 peak in Fig. 4A. These are both centered at higher energy than the diagonal, meaning that the two-quantum correlation is predominantly repulsive for the low-energy features.

We can rationalize the energetic ordering of optical transitions as follows. Given the local form of the exciton/exciton interaction, we solve the Schrödinger equation for the homogeneous 2D lattice model can using Greens function methods (10, 31), by assuming that the exciton/exciton interaction, U, is dipolar in nature and that the 2D Hamiltonian can be written in terms of either H-like or J-like single exciton operators (32). In Fig. 5, we show the slices through the 2D energy dispersion curves and sketches of biexciton wave functions for the HH (A and B) and JJ (C and D) cases. Here, we take the bare exciton energy E_x as the unit of energy and the lattice constant as the unit of length. We also take $t_H = -t_J$ and $U_H < 0$ for the HH biexciton and $U_J > 0$ for the JJ biexciton.

In Fig. 5 (A and C), corresponding to the 2H and 2J cases, respectively, the lower (solid blue) curve is the single exciton dispersion
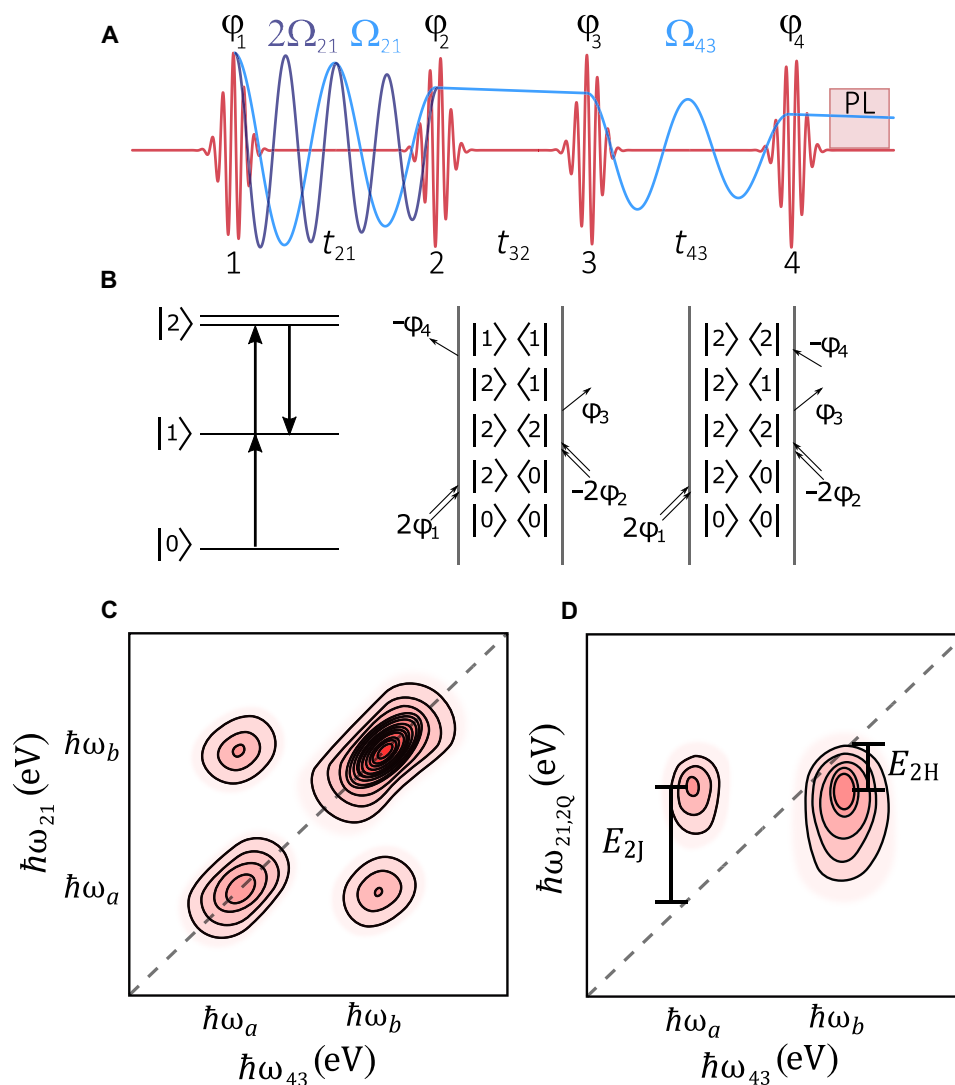
Fig. 3. 2D-PLE spectroscopy. (**A**) Schematic of the experimental pulse sequence. Here, ϕ_i is the phase of pulse $i = 1,2,3,4$. The interpulse delays are t_{21} (coherence time), t_{32} (population waiting time), and t_{43} (coherence time). The phase-modulation reference waveforms for phase-sensitive detection are generated optically at frequencies Ω_{21} and Ω_{43}, at which the relative phase $\phi_{21} = \phi_2 - \phi_1$ and $\phi_{43} = \phi_4 - \phi_3$ oscillate, respectively. In this work, time and spectrally integrated photoluminescence (PL) intensity are demodulated by phase-sensitive detection at the reference frequency $f_{ref} = \Omega_{43} + \Omega_{21}$ and $\Omega_{43} + 2\Omega_{21}$ for the one- and two-quantum correlation spectra, respectively, shown in Fig. 4. We outline in the Supplementary Materials that the 2D-PLE line shape can contain contributions from nonlinear incoherent population dynamics over the entire exciton lifetime and that all spectral line shapes presented in Fig. 4 are free from this undesired contribution under the excitation conditions of this experiment. (**B**) Double-sided Feynman diagrams of the two most important two-quantum response terms that couple a ground state ($|0\rangle$), a single exciton state ($|1\rangle$), and a two-exciton state ($|2\rangle$). (**C**) Schematic representation of the 2D-PLE expected spectrum for two correlated optical transitions at energies $\hbar\omega_a$ and $\hbar\omega_b$. The spectral axes $\hbar\omega_{21}$ and $\hbar\omega_{43}$ are obtained by Fourier transform of the 2D coherent PL decay function along time variables t_{21} and t_{43} at fixed t_{32}. (**D**) Schematic representation of a two-quantum 2D-PLE correlation spectrum. The two-quantum energy $\hbar\omega_{21,2Q}$ corresponds to the two-quantum coherences involving pulses 1 and 2. The diagonal line represents $\hbar\omega_{21,2Q} = 2\hbar\omega_{43}$.
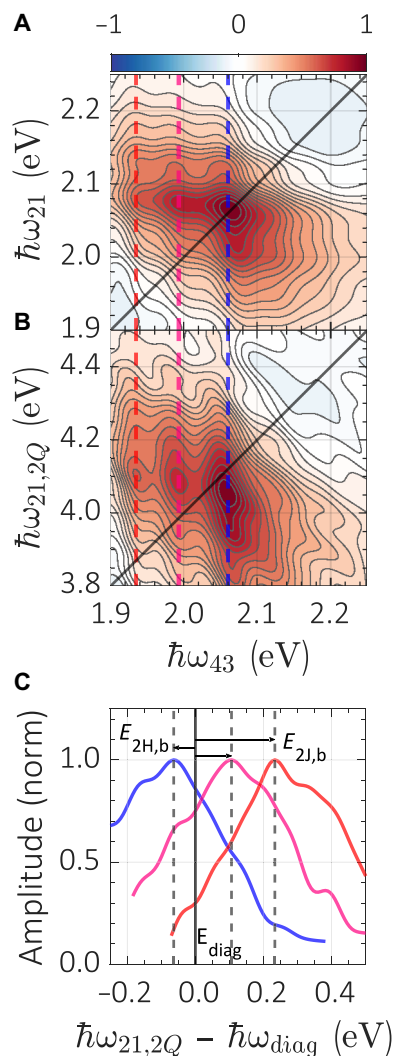
Fig. 4. 2D-PLE spectra measured at 5 K and t_{32} = 30 fs. (**A**) The real part of the one-quantum nonrephasing ($f_{ref} = \Omega_{43} + \Omega_{21}$) spectrum. (**B**) The real part of the two-quantum ($f_{ref} = \Omega_{43} + 2\Omega_{21}$) spectrum. (**C**) Spectral cuts along $\hbar\omega_{21,2Q} - \hbar\omega_{diag}$ spectral axis at fixed $\hbar\omega_{43} = 2.06$ (blue), 1.99 (fuchsia), and 1.94 eV (red) for the spectrum in (B). Here, $\hbar\omega_{diag}$ is the $\hbar\omega_{21,2Q} = 2\hbar\omega_{43}$ two-quantum diagonal energy, corresponding to zero net two-quantum correlation energy (neither binding nor repulsion). We chose to measure 2D coherent spectra with $t_{32} = 30$ fs to avoid ambiguous time ordering at $t_{32} = 0$. Because of the highly transient nature of the two-quantum coherence signal, it would not be possible to measure with $t_{32} \gg$ 30 fs (see the Supplementary Materials).

taken along the H or J directions, each referenced to twice the single H or J excitation energy. The upper (dashed green) curve is the corresponding two exciton dispersion for two free (unbound) excitons moving in the H or J directions. The solid (orange) corresponds to dispersion for the interacting biexciton but plotted along the perpendicular direction (i.e., k_J for the 2H and k_H for the 2J). The superimposed vertical arrows correspond to the excitations used to construct the double-sided Feynman diagrams for the nonlinear two-quantum coherence responses given in the SI, which generate coherences between the ground state and the free biexciton ($|0\rangle\langle 2X|$) and the ground state and the bound biexciton ($|0\rangle\langle b|$)

using the notation in the Supplementary Materials. This level scheme generates response functions consistent with those observed in our experiments.

Figure 5 (B and D) shows schematic sketches of the biexciton bound states as projected on to the 2D lattice. Pauli exclusion requires that a single site may not be doubly occupied, hence the nodal line in the middle of each. For the purely homogeneous model, the biexciton states are separable and can be written in terms of a traveling wave in one direction and a local bound state in the other.

In Fig. 4C, we display cuts of the two-quantum excitation spectrum at fixed one-quantum energies $\hbar\omega_{43}$. The cuts are along $\hbar\omega_{21,2Q}$ relative to the two-quantum diagonal energy $\hbar\omega_{diag}$. This is a good reference because signal on the diagonal corresponds to the energy of two excitons that coexist without interaction. We notice, on the one hand, that the 0-0 absorption peak, assigned to the vibronic progression of an H-aggregate (26), forms biexcitons with attractive interactions with $E_{2H, b} = -64 \pm 6$ meV, corresponding to the situation in which $t_{2Q, intra} < 0$, $U < 0$. On the other hand, the low-energy resonances, which we hypothesize to correspond to J-aggregate resonances, display predominantly repulsive two-quantum correlations, peaked at $E_{2J, b} = +106 \pm 6$ and $+233 \pm 6$ meV, respectively, which are produced when $t_{2Q, inter} > 0$, $U > 0$. This supports the hypothesis presented in Fig. 1 that both attractive and repulsive biexciton binding coexist within the inhomogeneously broadened 0-0 linear absorption peak. Using the experimentally determined $E_{2H, b}$, corresponding to the correlated biexciton at the origin of the H-aggregate progression, and the estimate of t_{inter} from its linear line shape in Fig. 2B, and under the hypothesis that $t_{inter} \sim t_{2Q, intra}$, we determine that $U/t_{2Q, intra} = 4.15$, placing the biexciton well into the range of stable biexcitons (see phase diagram in the Supplementary Materials). We find that while the scenario varies from sample to sample, this value is a lower limit, with an upper limit of 5.31. We acknowledge that the hypothesis of the similarity of the interchain exciton hopping integral with that associated with exciton-exciton interactions is highly speculative, but it does permit us to begin to develop a framework to understand the physical basis for Frenkel biexciton binding. For the biexciton associated with the J-aggregate, we do not have a direct measurement of t_{intra}, but we can speculate that it is a fraction of t_{inter} given the predominance of H-like character (25), placing J-like biexcitons also well within the stable (but unexpectedly repulsive) binding region, as depicted in Fig. 1. Our analysis thus brings forth new opportunities to explore U/t versus Δ/t phase diagrams for a broad class of molecular and macromolecular semiconductor materials, as portrayed in Fig. 1E and in the Supplementary Materials. For this, it is important to consider that U/t can be manipulated by chemical design and processing, while Δ/t is expected to depend predominantly on the chemical structure of the polymer repeat unit. Some comparisons can already be made. The work in (17) gives, for instance, values of $t = 80$ meV and $U/t \approx 4$ for epitaxially grown metal-halogen-phthalocyanine H-aggregates (fluoroaluminum phthalocyanine) based on transient absorption measurements; no bound biexcitons were observed in a similar J-aggregate system (chloroindium phthalocyanine).

DISCUSSION
In summary, the complex spectral structure due to hybrid HJ excitons (26) that are not resolved within the inhomogeneously broadened linear absorption line shape is revealed in a model polymeric
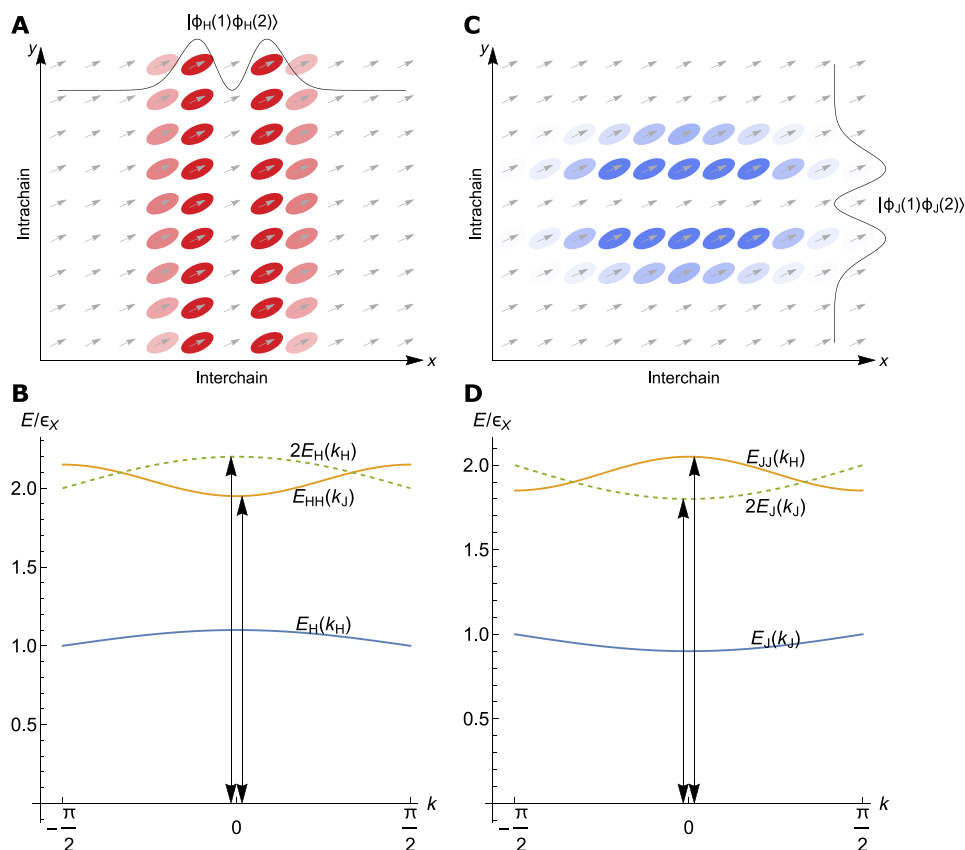
Fig. 5. Energy dispersion curves and sketches of biexciton wave functions. Wave functions for the HH (**A** and **B**) and JJ (**C** and **D**) cases. In (A) and (C), corresponding the 2H and 2J cases, respectively, the lower (solid blue) curve is the single exciton dispersion taken along the H or J directions. The upper (dashed green) curve is the corresponding two exciton dispersion for two free (unbound) excitons moving in the H or J directions. The solid (orange) line corresponds to dispersion for the interacting biexciton but plotted along the perpendicular direction (i.e., k_J for the 2H and k_H for the 2J). The wave functions sketched in (B) and (D) are the projections of the biexciton wave function probability density onto the 2D lattice. Pauli exclusion requires that a single site may not be doubly occupied, hence the nodal line.

semiconductor, PBTTT, using nonlinear coherent spectroscopy. All exciton resonances are identified along with their corresponding biexciton counterparts. A key finding is that interchain H-like excitons are associated with intrachain exciton-exciton couplings. In contrast, intrachain J-like excitons are paired by interchain exciton-exciton couplings. In either case, the biexciton binding energy is related to the exciton-exciton contact interaction U and the intersite hopping energy t, which are intrinsic molecular parameters quantified by quantum chemistry and that are expected to be controllable via chemical design and polymer assembly. The reason is that Δ and U depend on the local exciton dipole moment and thus likely on the strength of the push-pull character of the polymer building blocks, i.e., the chemistry of the monomer unit. The insights presented here thus enable prediction of the stability of Frenkel biexcitons in polymeric semiconductors and provide insights and design guidelines toward new materials discovery. More generally, it provides a platform to explore in unprecedented depth the many-body electronic structure of any material in which Frenkel excitons are the primary photoexcitations, ranging from organic semiconductors (33) and molecular crystals (34) to photosynthetic light-harvesting complexes (4) and protein/DNA structures (35).

MATERIALS AND METHODS
Sample preparation
PBTTT was synthesized as previously reported (M_n = 38 kg mol^{-1}, Đ$_M$ = 1.78) (22). PBTTT was dissolved in 1,2-dichlorobenzene (o-DCB; Sigma-Aldrich) at 85°C, and the solution was stirred for 1 hour. The concentration of the solution was 10 mg ml^{-1}. Films were drop-cast at 30°C on sapphire substrates (UQG Optics, 10 mm diameter and 1 mm thickness) from as-prepared solution and were subsequently left to dry at this temperature.

To corroborate the assignment of the 0-0 J-aggregate absorption energy, we processed blends of PBTTT with the ionic liquid bis(trifluoromethylsulfonyl)imide (Iolitec), with an ionic liquid ratio of 2 per repeating unit, in a solvent mixture consisting of o-DCB (Sigma-Aldrich) and cyclohexanone (Alfa Aesar) with a weight ratio of 4:6. The solutions were stirred at 110°C before casting. All chemicals described above were used without further purification. The films were cast from the solution on soda-lime glass slides at 80°C by wire-bar coating.

2D-PLE spectroscopy
The experimental setup shown schematically in the Supplementary Materials is derived from the phase-modulation and sensitive detection

technique previously developed by Marcus and co-workers (*30*) and has been described in previous publications (*36*, *37*). It implements a sequence of four collinear femtosecond pulses that are generated in two Mach-Zehnder interferometers (MZIs) that are nested in each arm of an outer MZI. Details are provided in the Supplementary Materials, including a detailed description of the experimental setup, a formal development of our approach for multiquantum coherence measurements.

DFT calculations

All DFT calculations were carried out with the Gaussian 16 (Revision A.03) software package (*38*), using the B3LYP hybrid functional and the 6-31G* basis set. The PBTTT chain was cut down into a trimer unit, and the hexadecyl side chains were replaced by ethyl groups to reduce the computational cost. The structure of oligomers was first optimized, and the ground-state dipole moment was obtained from single-point calculations. Excited states were calculated on top of the geometrical optimized structure using time dependent (TD)-DFT, and the excited-state dipole moment and transition dipole moment were retrieved from the results corresponding to the first excited state before relaxation. The results are visualized using Avogadro (*39*, *40*).

SUPPLEMENTARY MATERIALS

Supplementary material for this article is available at https://science.org/doi/10.1126/sciadv.abi5197

REFERENCES AND NOTES

1. J. Frenkel, On the transformation of light into heat in solids. I. *Phys. Rev.* **37**, 17–44 (1931).
2. V. M. Agranovich, B. S. Toshich, Collective properties of Frenkel excitons. *Sov. Phys. JETP* **26**, 104 (1968).
3. J. Keeling, S. Kéna-Cohen, Bose–Einstein condensation of exciton-polaritons in organic microcavities. *Annu. Rev. Phys. Chem.* **71**, 435–459 (2020).
4. G. D. Scholes, G. R. Fleming, A. Olaya-Castro, R. Van Grondelle, Lessons from nature about solar light harvesting. *Nat. Chem.* **3**, 763–774 (2011).
5. K. N. Avanaki, G. C. Schatz, Mechanistic understanding of entanglement and heralding in cascade emitters. *J. Chem. Phys.* **154**, 024304 (2021).
6. C. Silva, A. S. Dhoot, D. M. Russell, M. A. Stevens, A. C. Arias, J. D. MacKenzie, N. C. Greenham, R. H. Friend, S. Setayesh, K. Müllen, Efficient exciton dissociation via two-step photoexcitation in polymeric semiconductors. *Phys. Rev. B* **64**, 125211 (2001).
7. M. A. Stevens, C. Silva, D. M. Russell, R. H. Friend, Exciton dissociation mechanisms in the polymeric semiconductors poly (9, 9-dioctylfluorene) and poly (9, 9-dioctylfluorene-co-benzothiadiazole). *Phys. Rev. B* **63**, 165213 (2001).
8. C. Silva, D. M. Russell, A. S. Dhoot, L. M. Herz, C. Daniel, N. C. Greenham, A. C. Arias, S. Setayesh, K. Müllen, R. H. Friend, Exciton and polaron dynamics in a step-ladder polymeric semiconductor: The influence of interchain order. *J. Phys. Condens. Matter* **14**, 9803 (2002).
9. F. C. Spano, V. Agranovich, S. Mukamel, Biexciton states and two-photon absorption in molecular monolayers. *J. Chem. Phys.* **95**, 1400–1409 (1991).
10. G. Vektaris, A new approach to the molecular biexciton theory. *J. Chem. Phys.* **101**, 3031–3040 (1994).
11. F. Guo, M. Chandross, S. Mazumdar, Stable biexcitons in conjugated polymers. *Phys. Rev. Lett.* **74**, 2086–2089 (1995).
12. F. B. Gallagher, F. C. Spano, Theory of biexcitons in one-dimensional polymers. *Phys. Rev. B* **53**, 3790–3803 (1996).
13. S. Mazumdar, F. Guo, K. Meissner, B. Fluegel, N. Peyghambarian, Exciton-to-biexciton transition in quasi-one-dimensional organics. *J. Chem. Phys.* **104**, 9292–9296 (1996).
14. V. Agranovich, O. Dubovsky, D. Basko, G. La Rocca, F. Bassani, Kinematic frenkel biexcitons. *JOL* **85**, 221–232 (2000).
15. G. Kun, X. Shi-Jie, L. Yuan, Y. Sun, L. De-Sheng, Z. Xian, Effect of interchain coupling on a biexciton in organic polymers. *Chin. Phys. B* **18**, 2961–2966 (2009).
16. P. Xiang, M. Litinskaya, R. V. Krems, Tunable exciton interactions in optical lattices with polar molecules. *Phys. Rev. A* **85**, 061401 (2012).
17. A. Chakrabarti, A. Schmidt, V. Valencia, B. Fluegel, S. Mazumdar, N. Armstrong, N. Peyghambarian, Evidence for exciton-exciton binding in a molecular aggregate. *Phys. Rev. B* **57**, R4206–R4209 (1998).
18. V. I. Klimov, D. McBranch, N. Barashkov, J. Ferraris, Biexcitons in π-conjugated oligomers: Intensity-dependent femtosecond transient-absorption study. *Phys. Rev. B* **58**, 7654–7662 (1998).
19. K. W. Stone, D. B. Turner, K. Gundogdu, S. T. Cundiff, K. A. Nelson, Exciton-exciton correlations revealed by two-quantum, two-dimensional Fourier transform optical spectroscopy. *Acc. Chem. Res.* **42**, 1452–1461 (2009).
20. D. B. Turner, K. A. Nelson, Coherent measurements of high-order electronic correlations in quantum wells. *Nature* **466**, 1089–1092 (2010).
21. Y. Baba, G. Dujardin, P. Feulner, D. Menzel, Formation and dynamics of exciton pairs in solid argon probed by electron-stimulated ion desorption. *Phys. Rev. Lett.* **66**, 3269–3272 (1991).
22. I. McCulloch, M. Heeney, C. Bailey, K. Genevicius, I. MacDonald, M. Shkunov, D. Sparrowe, S. Tierney, R. Wagner, W. Zhang, M. L. Chabinyc, R. J. Kline, M. D. McGehee, M. F. Toney, Liquid-crystalline semiconducting polymers with high charge-carrier mobility. *Nat. Mater.* **5**, 328–333 (2006).
23. M. L. Chabinyc, M. F. Toney, R. J. Kline, I. McCulloch, M. Heeney, X-ray scattering study of thin films of poly(2,5-bis(3-alkylthiophen-2-yl) thieno[3,2-b]thiophene). *J. Am. Chem. Soc.* **129**, 3226–3237 (2007).
24. D. M. Delongchamp, R. J. Kline, Y. Jung, E. K. Lin, D. A. Fischer, D. J. Gundlach, S. K. Cotts, A. J. Moad, L. J. Richter, M. F. Toney, M. Heeney, I. McCulloch, Molecular basis of mesophase ordering in a thiophene-based copolymer. *Macromolecules* **41**, 5709–5715 (2008).
25. F. Paquin, H. Yamagata, N. J. Hestand, M. Sakowicz, N. Bérubé, M. Côté, L. X. Reynolds, S. A. Haque, N. Stingelin, F. C. Spano, C. Silva, Two-dimensional spatial coherence of excitons in semicrystalline polymeric semiconductors: Effect of molecular weight. *Phys. Rev. B* **88**, 155202 (2013).
26. F. C. Spano, C. Silva, H- and J-aggregate behavior in polymeric semiconductors. *Annu. Rev. Phys. Chem.* **65**, 477–500 (2014).
27. C. Hellmann, F. Paquin, N. D. Treat, A. Bruno, L. X. Reynolds, S. A. Haque, P. N. Stavrinou, C. Silva, N. Stingelin, Controlling the interaction of light with polymer semiconductors. *Adv. Mater.* **25**, 4906–4911 (2013).
28. J. Clark, J. F. Chang, F. C. Spano, R. H. Friend, C. Silva, Determining exciton bandwidth and film microstructure in polythiophene films using linear absorption spectroscopy. *Appl. Phys. Lett.* **94**, 163306 (2009).
29. J. Clark, C. Silva, R. H. Friend, F. C. Spano, Role of intermolecular coupling in the photophysics of disordered organic semiconductors: Aggregate emission in regioregular polythiophene. *Phys. Rev. Lett.* **98**, 206406 (2007).
30. P. F. Tekavec, G. A. Lott, A. H. Marcus, Fluorescence-detected two-dimensional electronic coherence spectroscopy by acousto-optic phase modulation. *J. Chem. Phys.* **127**, 214307 (2007).
31. E. N. Economou, *Green's Functions in Quanutm Physics* (Springer Series in Solid State Physics, Springer-Verlag, ed. 3, 2006).
32. E. R. Bittner, C. Silva-Acuña, Hybrid biexcitons in organic polymer aggregates: A case of Dr. Jekyl meeting Mr. Hyde. arXiv:2108.01618 (2021).
33. V. M. Agranovich, *Excitations in Organic Solids* (OUP Oxford, 2009), vol. 142.
34. N. J. Hestand, F. C. Spano, Molecular aggregate photophysics beyond the Kasha model: Novel design principles for organic materials. *Acc. Chem. Res.* **50**, 341–350 (2017).
35. E. R. Bittner, Lattice theory of ultrafast excitonic and charge-transfer dynamics in DNA. *J. Chem. Phys.* **125**, 094909 (2006).
36. E. Vella, H. Li, P. Grégoire, S. M. Tuladhar, M. S. Vezie, S. Few, C. M. Bázán, J. Nelson, C. Silva-Acuña, E. R. Bittner, Ultrafast decoherence dynamics govern photocarrier generation efficiencies in polymer solar cells. *Sci. Rep.* **6**, 29437 (2016).
37. P. Grégoire, E. Vella, M. Dyson, C. M. Bázán, R. Leonelli, N. Stingelin, P. N. Stavrinou, E. R. Bittner, C. Silva, Excitonic coupling dominates the homogeneous photoluminescence excitation linewidth in semicrystalline polymeric semiconductors. *Phys. Rev. B* **95**, 180201 (2017).
38. M. J. Frisch, G. W. Trucks, H. B. Schlegel, G. E. Scuseria, M. A. Robb, J. R. Cheeseman, G. Scalmani, V. Barone, G. A. Petersson, H. Nakatsuji, Gaussian 16 Revision A.03 (Gaussian Inc., 2016).
39. A. Chemistry, Avogadro: An open-source molecular builder and visualization tool, version 1.2.0.
40. M. D. Hanwell, D. E. Curtis, D. C. Lonie, T. Vandermeersch, E. Zurek, G. R. Hutchison, Avogadro: An advanced semantic chemical editor, visualization, and analysis platform. *J. Chem.* **4**, 17 (2012).